Magnetism in amorphous transition metals. II.

Y. Kakehashi
Department of Physics, Hokkaido Institute of Technology, Maeda, Teine-ku, Sapporo 006, Japan
(Received 31 December 1991; revised manuscript received 13 October 1992)

Susceptibilities and pressure effects on the magnetic properties of amorphous transition metals have been investigated on the basis of a finite-temperature theory of local-environment effects in amorphous metallic magnetism. Calculated high-field susceptibilities, paramagnetic susceptibilities, effective Bohr-magneton numbers, and the pressure dependence of magnetization, Curie temperature, and spin-glass temperatures are shown to explain various aspects of the magnetism in amorphous and liquid transition metals and alloys as a function of the d electron number. It is demonstrated that these quantities are governed by the electronic structure of amorphous transition metals, in particular, by the main-peak position in the noninteracting density of states for amorphous structure. Moreover, the detailed investigations for susceptibilities, forced-volume magnetostriction, and the T-P phase diagram in the reentrant spin-glass region reveal that the itinerant-electron spin glasses in the Fe-rich amorphous alloys with more than 90 at. % Fe are caused by structural disorder instead of configurational disorder.

I. INTRODUCTION

Basic properties of amorphous metallic magnetism have remained unsolved for many years because it was very difficult to extract the essential part from the experimental data of amorphous magnetic alloys.[1-4] Early data of amorphous transition-metal alloys containing considerable amount of metalloids,[3] for example, have been considered to show that the effect of structural disorder is simply to reduce the magnetizations and Curie temperatures (T_C), while recent experimental data for Fe-rich amorphous alloys with less than 10 at. % early transition metals[4-7] indicate a complete disappearance of ferromagnetism and a formation of the spin-glass (SG) phase. The recent data of amorphous Co_cY_{1-c}($0.6 \leq c \leq 0.9$) alloys[8] suggest an enhancement of the Curie temperature of amorphous pure Co by 450 K in contradiction to the early picture obtained from the amorphous transition-metalloid alloys.

In a previous paper (which is referred to as I),[9] we have developed a theory of amorphous metallic magnetism that takes into account both the thermal spin fluctuations and the fluctuations of local magnetic moments (LM) with respect to the structural disorder. The theoretical investigations have revealed the basic property of magnetism in amorphous transition metals; the SG for $6.7 \lesssim N \lesssim 7.2$, cluster SG for $7.2 \lesssim N \lesssim 7.35$, reentrant SG for $7.35 \lesssim N \lesssim 7.385$, and the ferromagnetism for $7.385 \lesssim N \lesssim 9.0$, where N denotes the d electron number per atom. The enhancement of T_C due to structural disorder was also found in the range $7.9 \lesssim N \lesssim 8.5$. These theoretical results support the recent experimental data for Fe-rich[4] and Co-rich[8] amorphous alloys with nonmagnetic early transition metals. Moreover, the electronic structure inherent in the amorphous structure was shown to be reflected in these magnetic properties.

In the present paper, we investigate a systematic variation of susceptibilities and pressure effects on the magnetization, T_C, and the SG temperature (T_g) in amorphous $3d$ transition metals with use of the same approach. We clarify in more detail the physical picture obtained in paper I. In particular, we will show that the systematic change of these quantities in $3d$ series is governed by the main-peak position in the noninteracting densities of states (DOS).

In Sec. II, we briefly review the finite-temperature theory of local environment effect (LEE) in amorphous metallic magnetism. In Sec. III, we present numerical results for susceptibilities as a function of d electron number and temperature. The differences in susceptibilities between the bcc, fcc, and amorphous structures will be discussed in comparison with the experimental data of fcc and liquid transition-metal alloys.

Pressure effects on the magnetization, Curie temperature, and SG temperature are discussed in Sec. IV. We will explain the large negative $\partial T_C/\partial p$ near amorphous and the suppression of $\partial T_C/\partial p$ near the ferromagnetic instability for the fcc and amorphous structures. One of the most important topics on the amorphous itinerant magnetism is the anomalous magnetic-field and pressure effects in the reentrant SG region. We discuss these effects in more details in Sec. V, in particular, the anomalous forced volume magnetorestriction as seen in Fe-rich Fe-Zr amorphous alloys[10] and the T-p phase diagram as found in Fe-La amorphous alloys.[11] A part of this section has been published as a letter.[12] Finally, we summarize our numerical results in Sec. VI.

II. FINITE-TEMPERATURE THEORY OF LEE

We adopt the degenerate-band Hubbard model with a Hund's rule coupling, and make use of the functional integral method to take into account the thermal spin fluctuations.[13] The method exactly transforms the interacting Hamiltonian into a one-electron Hamiltonian with the time-dependent random exchange fields acting on

 ©1993 The American Physical Society

each site. Within the static approximation which neglects the time dependence of the field variables, the central local moment is expressed as a classical average of the field variable ξ on the same site with respect to a free-energy functional.

We next introduce an effective medium $\mathcal{L}_\sigma^{-1}$ describing the thermal spin fluctuations into the diagonal part of the one-electron Hamiltonian, and expand the deviation from the effective medium in the energy functional with respect to the site. After making use of a molecular-field type of approximation for the surrounding field variables, we obtain an expression for the thermal average of the central local moment as follows:[14]

$$\langle m_0 \rangle = \langle \xi \rangle = \frac{\int d\xi\, \xi e^{-\beta\Psi(\xi)}}{\int d\xi\, e^{-\beta\Psi(\xi)}} \ . \tag{2.1}$$

Here β denotes the inverse temperature.

The energy functional $\Psi(\xi)$ in Eq. (2.1) consists of the single-site energy $E(\xi)$, the atomic pair energies $\Phi_{0j}^{(a)}(\xi)$, and the exchange pair energies $\Phi_{0j}^{(e)}(\xi)$ in the effective medium:

$$\Psi(\xi) = E(\xi) + \sum_{j=1}^{z} \left[\Phi_{0j}^{(a)}(\xi) - \Phi_{0j}^{(e)}(\xi) \frac{\langle m_j \rangle}{x_j} \right] , \tag{2.2}$$

$$E(\xi) = \int d\omega f(\omega) \frac{D}{\pi} \mathrm{Im} \sum_\sigma \ln[L_\sigma^{-1}(\xi) - \mathcal{L}_\sigma^{-1} + F_{00\sigma}^{-1}] - N w_0(\xi) + \tfrac{1}{4}\tilde{J}\xi^2 , \tag{2.3}$$

$$\begin{bmatrix} \Phi_{0j}^{(a)}(\xi) \\ \Phi_{0j}^{(e)}(\xi) \end{bmatrix} = \frac{1}{2} \sum_{\nu=\pm} \begin{bmatrix} 1 \\ -\nu \end{bmatrix} \Phi_{0j}(\xi, \nu x_j) , \tag{2.4}$$

$$\Phi_{0j}(\xi, \nu x_j) = \int d\omega f(\omega) \frac{D}{\pi} \mathrm{Im} \sum_\sigma \ln[1 - F_{0j\sigma} F_{j0\sigma} \tilde{t}_{0\sigma}(\xi) \times \tilde{t}_{j\sigma}(\nu x_j)] , \tag{2.5}$$

$$\tilde{t}_{j\sigma}(\xi) = \frac{L_{j\sigma}^{-1}(\xi) - \mathcal{L}_\sigma^{-1}}{1 + [L_{j\sigma}^{-1}(\xi) - \mathcal{L}_\sigma^{-1}] F_{jj\sigma}} \ . \tag{2.6}$$

Here the summation on the right-hand side (rhs) in Eq. (2.2) is taken over $z(=12)$ atoms on the well-defined nearest-neighbor (NN) shell. We have neglected the couplings between further distant atoms because of the rapid damping in the disordered systems with increasing interatomic distance.[15] $\langle m_j \rangle$ and x_j are the thermal average and amplitude of the LM on the neighboring site j. $f(\omega)$ in Eqs. (2.3) and (2.5) denotes the Fermi distribution function. D, N, and $\tilde{J}$ are the number of orbital degeneracies ($D=5$), d electron number, and the effective exchange-energy parameter, respectively. The charge potential $w_j(\xi)$ in Eq. (2.3) is determined from the charge neutrality condition on each site j. The locator for σ spin electrons $L_{j\sigma}$ in Eqs. (2.3) and (2.6) is defined by

$$L_{j\sigma}^{-1}(\xi) = \omega + i\delta - \epsilon^0 - w_j(\xi) + \tfrac{1}{2}\tilde{J}\xi\sigma + h\sigma + \mu , \tag{2.7}$$

where $\epsilon^0 - \mu$ is the atomic level measured from the chemical potential μ, h is a uniform magnetic field in units of $g\mu_B$, δ is an infinitesimal positive number.

Structural disorder appears in Eqs. (2.3) and (2.5) via the coherent Green function defined by

$$F_{ij\sigma} = [(\mathcal{L}_\sigma^{-1} - t)^{-1}]_{ij} , \tag{2.8}$$

where t denotes the transfer-integral matrix t_{ij}.

In the present theory the diagonal coherent Green functions on the NN shell are approximated by their structural average:

$$[F_{jj\sigma}]_s = F_\sigma = \int \frac{[\rho(\epsilon)]_s}{\mathcal{L}_\sigma^{-1} - \epsilon} d\epsilon \ . \tag{2.9}$$

Here $[\ ]_s$ means the structural average, $\rho(\epsilon)$ is the density of states for noninteracting electrons in amorphous metals.

The coherent Green functions $F_{00\sigma}$ and $F_{0j\sigma}$ $(=F_{j0\sigma})$ are obtained by making use of the Bethe approximation:

$$F_{00\sigma} = \left[\mathcal{L}_\sigma^{-1} - \frac{\sum_{i=1}^{z} t_{i0}^2}{\mathcal{L}_\sigma^{-1} - \mathcal{S}_\sigma} \right]^{-1} , \tag{2.10}$$

$$F_{0j\sigma} = \frac{t_{j0}}{\mathcal{L}_\sigma^{-1} - \mathcal{S}_\sigma} F_{00\sigma} \ . \tag{2.11}$$

Here the self-energy $\mathcal{S}_\sigma$ describes an effective medium due to the structural disorder.

Equation (2.1) manifests that the central LM is determined by the surrounding LM's $\{\langle m_j \rangle\}$ and the squares of the transfer integrals $\{t_{j0}\}$. These quantities have distributions $g(\langle m_j \rangle)$ and $p_s(y_j)$ in the amorphous systems, where $y_j = t_{j0}^2 - [t_{j0}^2]_s$. The distribution of the central LM is then obtained from $g(\langle m_j \rangle)$ and $p_s(y_j)$ via Eq. (2.1). Since it should be identical with the surrounding ones, we obtain an integral equation for the distribution function as follows:[14,16]

$$g(M) = \int \delta(M - \langle m_0 \rangle) \prod_{j=1}^{z} [p_s(y_j) dy_j g(m_j) dm_j] \ . \tag{2.12}$$

By making use of the decoupling approximation on the rhs of Eq. (2.12), which is correct up to the second moment, we obtain the self-consistent equations for $[\langle m \rangle]_s$ and $[\langle m \rangle^2]_s$:

$$\begin{bmatrix} [\langle m \rangle]_s \\ [\langle m \rangle^2]_s \end{bmatrix} = \sum_{n=0}^{z} \Gamma(n, z, \tfrac{1}{2}) \times \sum_{k=0}^{n} \sum_{l=0}^{z-n} \Gamma(k, n, q) \Gamma(l, z-n, q) \times \begin{bmatrix} \langle \xi \rangle_{nkl} \\ \langle \xi \rangle_{nkl}^2 \end{bmatrix} , \tag{2.13}$$

$$\langle \xi \rangle_{nkl} = \frac{\int d\xi\, \xi e^{-\beta\Psi_{nkl}(\xi)}}{\int d\xi\, e^{-\beta\Psi_{nkl}(\xi)}} , \tag{2.14}$$

$$\Psi_{nkl}(\xi)=E_n(\xi)+n\Phi^{(a)}_{-n}(\xi)+(z-n)\Phi^{(a)}_{+n}(\xi) -[(2k-n)\Phi^{(e)}_{-n}(\xi) +(2l-z+n)\Phi^{(e)}_{+n}(\xi)]\frac{[\langle m\rangle^2]^{1/2}_s}{x}\ , \quad (2.15)$$

$$q=\frac{1}{2}\left[1+\frac{[\langle m\rangle]_s}{[\langle m\rangle^2]^{1/2}_s}\right]\ . \quad (2.16)$$

In the present approximation the atomic local environment is described by a contraction or a stretch of the NN atoms by $[(\delta R)]^{1/2}_s$. Both atomic and spin configurations on the NN shell are expressed by the binomial distribution function $\Gamma(k,n,q)$ defined by $[n!/k!(n-k)!]q^k(1-q)^{n-k}$. Thus, the LM $\langle\xi\rangle_{nkl}$ and energy $\Psi_{nkl}(\xi)$ are specified by n (the number of contracted atoms on the NN shell), k (the number of up spins on the contracted atoms), and l (the number of up spins on the z-n stretched atoms). Associated energy functionals $E_n(\xi)$ and $\Phi^{(a)}_{+n}(\xi)$ $[\Phi^{(a)}_{-n}(\xi)]$ in Eq. (2.15) mean the single-site energy and the atomic pair energy for the contracted (stretched) pair in the local environment n. The exchange pair energies $\Phi^{(e)}_{\pm n}(\xi)$ are defined in the same way.

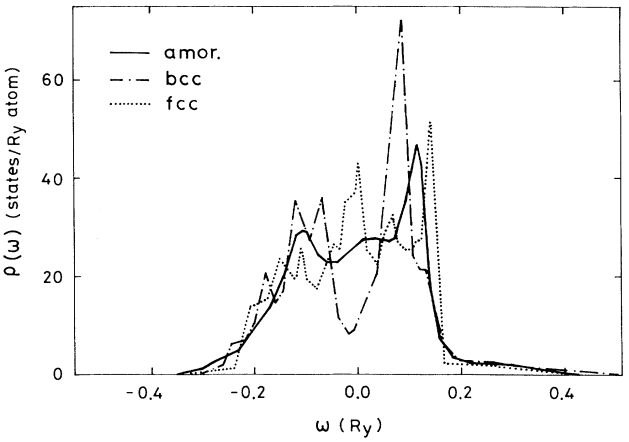

FIG. 1. The input density of states (DOS) for the amorphous (solid curve) (Ref. 23), bcc (dot-dashed curve) (Ref. 23), and fcc (dotted curve) structures (Ref. 24).

The energy functionals $\Psi_{nkl}(\xi)$ include unknown effective mediums, $\mathcal{S}_\sigma$ and $\mathcal{L}^{-1}_\sigma$. The former is determined so that the structural average of $F_{00\sigma}$ [Eq. (2.10)] is equal to the exact one [Eq. (2.9)]:

$$\sum_{\nu=\pm}\frac{1}{2}\left[\mathcal{L}^{-1}_\sigma-z[t^2_{j0}]_s\left[1+\nu\frac{[(\delta t^2_{j0})^2]^{1/2}_s}{\sqrt{z}\,[t^2_{j0}]_s}\right](\mathcal{L}^{-1}_\sigma-\mathcal{S}_\sigma)^{-1}\right]^{-1}=F_\sigma\ . \quad (2.17)$$

Here the average transfer integral $[t^2_{j0}]_s$ is obtained from the input DOS as follows:

$$z[t^2_{j0}]_s=\int(\epsilon-\epsilon_0)^2[\rho(\epsilon)]_s d\epsilon\ . \quad (2.18)$$

The ratio $[(\delta t^2_{j0})^2]^{1/2}_s/[t^2_{j0}]_s$ is related with the fluctuation of the NN atomic distance as follows:

$$[(\delta t^2_{j0})^2]_s/[t^2_{j0}]_s=2\kappa\frac{[(\delta R)^2]^{1/2}_s}{[R]_s}\ . \quad (2.19)$$

Here the relation $t(R)\propto R^{-\kappa}$ is adopted.

The effective medium $\mathcal{L}^{-1}_\sigma$ is determined from the CPA (coherent-potential approximation) condition:[17-18]

$$\sum_\nu\frac{1}{2}\left[1+\nu\frac{[\langle\xi\rangle]_s}{[\langle\xi^2\rangle]^{1/2}_s}\right]\{L^{-1}_\sigma(\nu[\langle\xi^2\rangle]^{1/2}_s)-\mathcal{L}^{-1}_\sigma+F^{-1}_\sigma\}^{-1}=F_\sigma\ . \quad (2.20)$$

Since $[\langle\xi\rangle]_s$ and $[\langle\xi^2\rangle]_s$ in Eq. (2.20) include again $[\langle m\rangle]_s$ and $[\langle m\rangle^2]_s$ via Eqs. (2.15) and (2.16), one has to solve Eqs. (2.13), (2.17), and (2.20) self-consistently to obtain $[\langle m\rangle]_s$, $[\langle m\rangle^2]_s$, $\mathcal{S}_\sigma$, and $\mathcal{L}^{-1}_\sigma$.

The theory describes the itinerant electron SG ($[\langle m\rangle]_s=0$ and $[\langle m\rangle^2]_s\neq 0$). The transition temperature T_g has been shown to reduce to the well-known formula $T_g=\sqrt{z}\,|\mathcal{J}|$ in the LM limit and the $\pm\mathcal{J}$ model.[19,20] Here $\mathcal{J}$ denotes the exchange coupling constant between the LM's.

The input parameters are the d electron number N, the effective exchange-energy parameter $\tilde{J}$, the DOS $[\rho(\epsilon)]_s$, and the fluctuation of the interatomic distance $[(\delta R)^2]^{1/2}_s/[R]_s$. In the following numerical calculations we adopted $[(\delta R)^2]^{1/2}_s/[R]_s=0.06$, which is consistent with those estimated from the width of the first peak in the theoretical[21] and experimental[22] pair-distribution functions for amorphous Fe. The input DOS's are presented in Fig. 1. It is essential for the magnetism in amorphous transition metals that the main peak for the amorphous DOS is located just between the bcc and fcc ones.

III. SUSCEPTIBILITIES

Magnetic susceptibilities are one of the most basic properties in magnetism. We present here the high-field susceptibility as well as the paramagnetic susceptibility, which are obtained from the numerical derivative of magnetization with respect to the magnetic field. We adopted here the input parameters for amorphous Fe ($\tilde{J}=0.059\,045$ Ry) and the input DOS as shown in Fig. 1,

and changed the d electron number N to examine a general trend in $3d$ series.

Calculated high-field susceptibilities χ_{HF} near the ferromagnetic instability are presented in Fig. 2 as a function of the d electron number. Amorphous transition metals show the SG ferromagnet transition at a critical electron number $N_c = 7.364$ for the present choice of parameters with increasing d electron number. The susceptibility shows there an asymmetric divergence. Large χ_{HF}'s in the SG region are attributed to the frustrated LM's. Although the magnitudes of calculated χ_{HF} are comparable to the experimental data,[4] the asymmetric behavior has not yet been verified, since the SG region realized in the Fe-rich amorphous alloys is very narrow. A remarkable point is that χ_{HF}'s for an amorphous structure are much larger than those for the bcc and fcc structures even if the d electron number is considerably deviated from N_c. [Note that χ_{HF}'s are 1.118×10^2 μ_B/Ry atom for bcc Fe, 1.114×10^2 μ_B/Ry atom for hcp Co, and 0.496×10^2 μ_B/Ry atom for fcc Ni at 4.2 K (Ref. 25).] This is because the susceptibilities for an amorphous structure are accompanied with the reversal of the LM's which are weakly coupled to the surrounding LM's due to the structural disorder.

The susceptibilities at high temperatures are presented in Fig. 3 for three structures as a function of the d electron number. The fcc susceptibility shows the highest value among the amorphous, bcc, and fcc structures for $5.0 \lesssim N \lesssim 5.85$ and $8.55 \lesssim N \lesssim 9.43$, the bcc one for $5.85 \lesssim N \lesssim 7.98$, and the amorphous one for $7.98 \lesssim N \lesssim 8.55$ and $9.43 \lesssim N < 10.0$. Although there is no simple relation between the noninteracting DOS and susceptibilities at finite temperatures because of the large thermal spin fluctuations, we find a correlation between the differences in susceptibilities $\Delta\chi$ and the main-peak positions of the noninteracting DOS, as found for magnetization and T_C in paper I. In fact, the d electron number $N^* = 7.440$ has a Fermi level at the main-peak position for the bcc structure. The bcc susceptibility takes the highest value near there among three structures. This

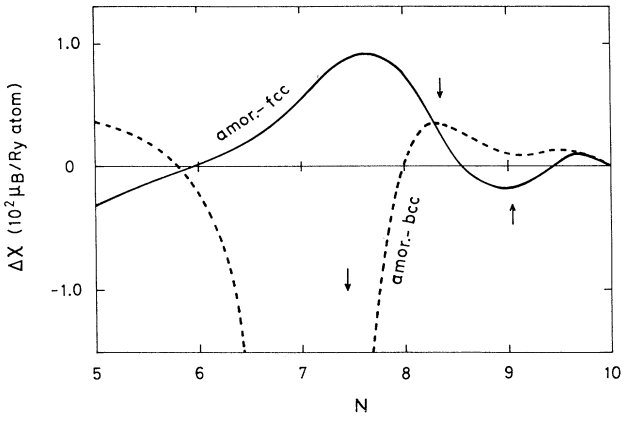

FIG. 3. Relative paramagnetic susceptibilities of amorphous and bcc structures (dashed curve), and amorphous and fcc structures (solid curves) calculated at 2400 K. Arrows indicate the d electron numbers N^* with the Fermi level at the main peak for each structure.

implies that the susceptibility enhancement associated with a large magnetic gain due to the main peak at the Fermi level remains even above T_C. In the same way, we find the highest value of the amorphous susceptibility near $N^* = 8.352$ with the main peak at the Fermi level, and that of the fcc susceptibility near $N^* = 9.048$. The enhancement of the fcc susceptibility near $N = 5.0$ is also attributed to a large peak near the center of gravity for the fcc DOS in Fig. 1.

There is no direct experimental data which support our results for $\Delta\chi$ at the present stage. However, we note that our results are consistent with the data[26] for liquid transition-metal alloys as shown in Fig. 4, if we assume that the amorphous structure is similar to the liquid one.

The temperature variations of the paramagnetic susceptibilities for amorphous structure are presented in Fig. 5. The susceptibilities χ follow the Curie-Weiss law (CW)

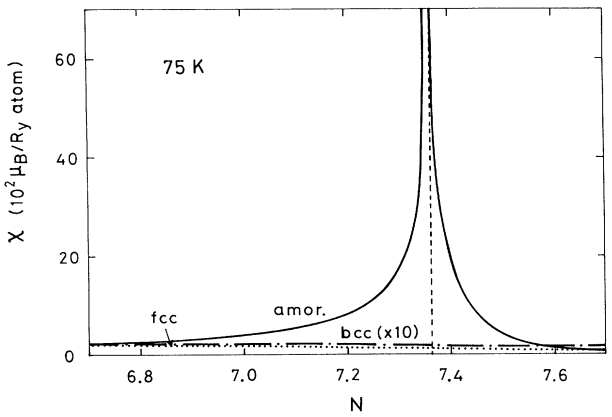

FIG. 2. High-field susceptibilities (χ_{HF}) as the function of the d electron numbers (N) for the amorphous (solid curve), bcc (dot-dashed curve), and fcc (dotted curve) structures. Note that the bcc susceptibilities are multiplied by a factor of 10.

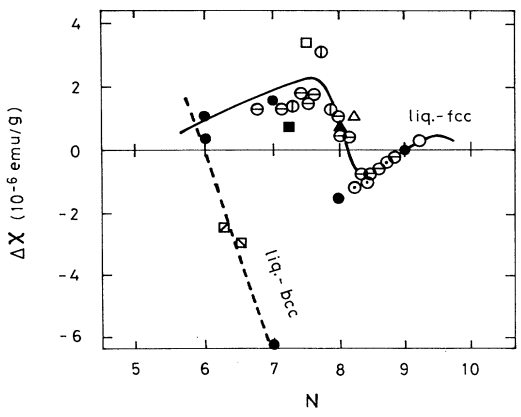

FIG. 4. Susceptibility changes at the melting point for $3d$ transition-metal alloys (Ref. 26). ●: Mn, Fe, Co, and Ni; ○: Ni-Cu; ⊙: Co-Ni; ⊖: Fe-Mn, Fe-Ni; ⊕: Fe-Co; △: Ni-Mn; ▲: Ni-Cr; □: Co-Mn; ■: Co-Cr; ⊠: Fe-Cr; ⊠: Fe-V.

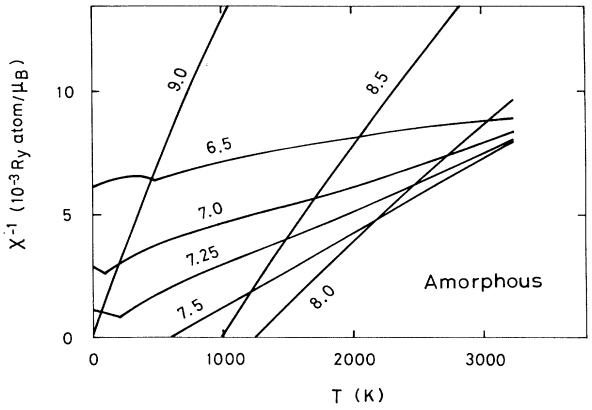

FIG. 5. Inverse paramagnetic spin susceptibilities for amorphous transition metals with $\tilde{J}=0.059\,045$ Ry and input DOS in Fig. 1.

above about 1500 K irrespective of the structures. Below 1000 K, the deviation from the CW law is seen in some cases as shown in Fig. 6. The bcc susceptibility for $N=8.5$ (dot-dashed line in Fig. 6), for example, shows the Pauli paramagnetic behavior below 1000 K because of the small DOS at the Fermi level [$\tilde{J}\rho(0)/2=0.69$], although the susceptibility follows the CW law above 2000 K since the LM's are induced with increasing temperature. Similar behavior is also seen in the fcc susceptibility for $N=8.5$ (dotted line in Fig. 6), where $\tilde{J}\rho(0)/2=1.01$.

The amorphous susceptibilities for $N=6.5$, 7.0, and 7.25 show the cusp at T_g. The inverse susceptibilities are upwards convex above T_g. This is not due to the structural disorder, but seems to be a behavior characteristic of the close-packed systems since it is also seen in the fcc χ^{-1}.

We have calculated the effective Bohr-magneton numbers ($m_{\rm eff}$) for three types of structures from the high-temperature susceptibilities. The results for Fe, Co, and Ni are summarized in Table I. Theoretical values are underestimated by 25% as compared with the experimental ones because of the neglect of the transverse spin fluctuations and overestimation of itinerant character in the static approximation with the effective exchange-energy parameter $\tilde{J}$. Nevertheless, previous investigations for the substitutional $3d$ transition-metal alloys[29] revealed that the present theory describes a systematic change of $m_{\rm eff}$ as a function of N. Figure 7 shows such a change of $m_{\rm eff}$ for three types of structures.

TABLE I. Calculated effective Bohr-magneton number (μ_B) for Fe [$N=7.0$, $\tilde{J}=0.059\,045$ Ry, and W(Fe) in Fig. 1], Co [$N=8.1$, $\tilde{J}=0.090$ Ry, and W(Co)/W(Fe)$=0.441/0.393$], and Ni [$N=9.1$, $\tilde{J}=0.060$ Ry, and W(Ni)/W(Fe)$=0.364/0.393$]. Experimental values are shown in parentheses.

	Fe	Co	Ni
amor	3.55	1.96	1.27
bcc	2.40 (3.20)[a]	2.24	1.37
fcc	4.54 (6.16)[b]	2.32 (3.15)[c]	1.26 (1.61)[a]

[a]Sucksmith and Pearce, Ref. 27.
[b]Renz and Methfessel, Ref. 30.
[c]Fallot, Ref. 28.

The effective Bohr-magneton numbers increase with decreasing d electron number from $N=10$ to 5. It is seen that the region where each structure takes the minimum value among three $m_{\rm eff}$'s corresponds well to the d electron number (N^*) with the main peak at the Fermi level in the noninteracting DOS for each structure. This is because the strong ferromagnetism caused by the main peak for each structure leads to small $m_{\rm eff}$ which is close to the amplitudes of LM's. When the d electron numbers decrease from N^*, the effective Bohr-magneton numbers increase gradually because of the change of magnetism from the strong to the weak one. The fcc $m_{\rm eff}$ first increases rapidly from $N=8.5$, the amorphous $m_{\rm eff}$ increases next from $N=8.0$, and finally the bcc $m_{\rm eff}$ increases from $N=6.5$ according to the inequality $N^*(\text{bcc})<N^*(\text{amor})<N^*(\text{fcc})$. The experimental data of $m_{\rm eff}$ in the fcc and liquid transition-metal alloys by Renz

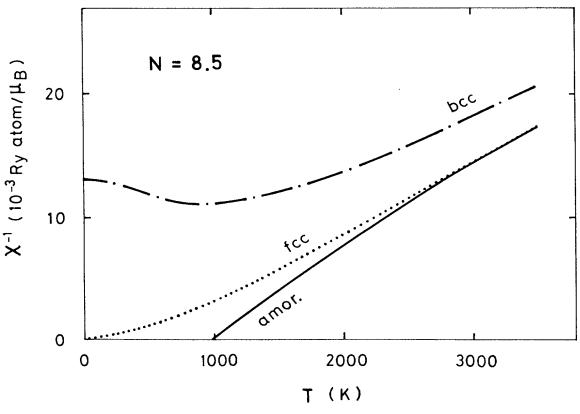

FIG. 6. Temperature dependence of the inverse paramagnetic susceptibilities for $N=8.5$.

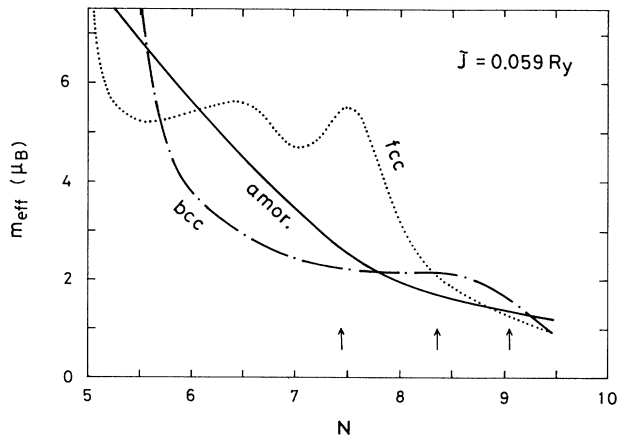

FIG. 7. Effective Bohr-magneton numbers calculated around $T=1800$ K. Arrows indicate N^*.

and Methfessel[30] show that the fcc m_{eff} rapidly increase as compared with the liquid ones with decreasing N from 8.5 to 7.0. This behavior may be regarded as a supporting evidence.

IV. PRESSURE EFFECTS

A. Pressure dependence of magnetization

We calculated the pressure dependence of magnetizations by taking the numerical derivative of $M=[\langle m\rangle]_s$ with respect to the volume. We assumed Heine's law, $t(R)\propto R^{-\kappa}$ (with $\kappa=3.8$) and $\tilde{J}=$const.[31] The results for Fe, Co, and Ni are given in Table II. The present theory explains the qualitative aspect of $\partial M/\partial p$, but does not give quantitative agreement with the experimental data since $\partial M/\partial p$ is sensitive to the DOS at the Fermi level.

The d electron number dependence of $B\partial M/\partial p$ is presented in Fig. 8. Here B denotes the bulk modulus. Small $\partial M/\partial p$ are obtained near N^* for each structure, which is a characteristic of the strong ferromagnetism. In particular, the amorphous $\partial M/\partial p$ is small around $N^*=8.35$, where the bcc and fcc structures show a large $\partial M/\partial p$ associated with the ferromagnetic instability. This trend is seen in the experimental data for Fe-Ni alloys[35-37] as shown in Fig. 9.

B. Pressure dependence of T_C and T_g

The pressure dependences of the Curie and SG temperatures were also obtained numerically by taking the derivative $\partial T_C/\partial V$ with respect to the volume V. The results are shown in Fig. 10 as a function of N for three types of structures.

Before we discuss the effects of structural disorder on $\partial T_C/\partial p$, we remark on the following points. First, the present theory overestimates the volume dependence of T_C generally because of the overestimate of the itinerant-electron character in the static approximation with effective exchange-energy parameters. Correlation effects at finite temperatures reduce the itinerant character, as shown by the Gutzwiller-type variational theory at finite temperatures.[38,39] (See the change of sign of $\partial T_C/\partial p$ for Ni in Fig. 10.) Second, the calculated $\partial T_C/\partial p$ are considerably sensitive to the shape of input DOS as seen by comparing the present results with the previous ones obtained from the less realistic DOS.[39] The present results therefore stand for qualitative ones.

TABLE II. Pressure dependence of the magnetization $B\partial M/\partial p$ (μ_B) for Fe, Co, and Ni.

Element	Fe		Co		Ni
Structure	bcc	amor	bcc	fcc	fcc
Calc. (150 K)	−1.83	−0.73	−0.66	−0.46	−0.31
Expt. (300 K)	−1.02[a]			−0.72[b]	−0.30[c]

[a]Kouvel and Wilson, Ref. 32.
[b]Kouvel and Hartelius, Ref. 33.
[c]Ebert and Kusmann, Ref. 34.

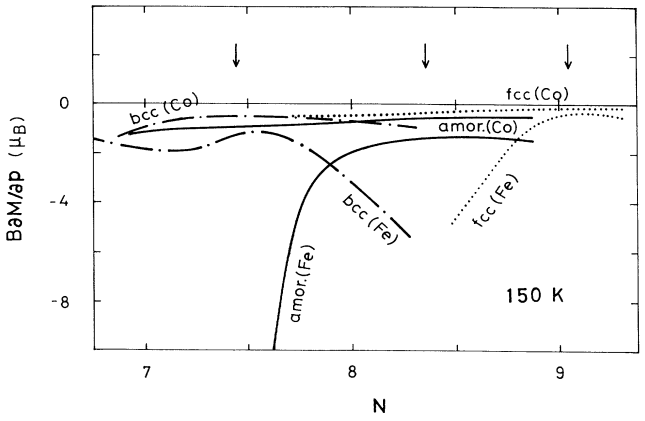

FIG. 8. Calculated pressure dependences of magnetizations as a function of the d electron number N. The results are shown for two sets of input parameters, Fe [$\tilde{J}=0.059\,045$ Ry and the band width W(Fe) in Fig. 1] and Co [$\tilde{J}=0.090$ Ry and $W(\text{Co})/W(\text{Fe})=0.441/0.393$]. Arrows indicate the d electron numbers with the Fermi level at the main peak in the input DOS for each structure.

Calculated $|\partial T_C/\partial p|$ take small values in the strong ferromagnetic region near N^*, while they become larger when the d electron number deviates from N^*. This means that the basic electronic structures shown in Fig. 1 are again reflected in $\partial T_C/\partial p$. The difference in the main-peak position between the amorphous and fcc DOS's corresponds to the electron number difference $\Delta N^*=N^*(\text{fcc})-N^*(\text{amor})=0.695$. This difference explains why the Invar anomalies in the amorphous transition-metal alloys[39-41] occur around $N=7.0$ instead of $N=7.7$. Theoretical results seem to be consistent with the experimental data[36-37,42] shown in Fig. 11, where $\partial T_C/\partial p(\text{amor})<\partial T_C/\partial p(\text{fcc})$ at $N\approx 9.0$ and $\partial T_C/\partial p(\text{amor})>\partial T_C/\partial p(\text{fcc})$ at $N\approx 7.0$.

Present theory describes the suppression of $\partial T_C/\partial p$ near the ferromagnet SG transition. This is caused by

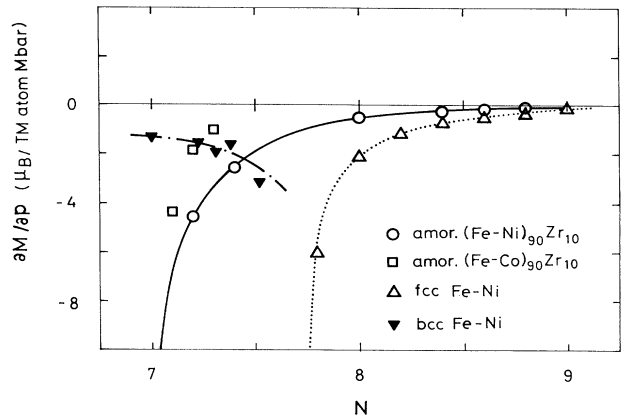

FIG. 9. Experimental data of the pressure dependence of magnetizations for amorphous and crystalline alloys at $T=4.2$ K as a function of the average d electron number for the $3d$ transition-metal elements (Refs. 35 and 36).

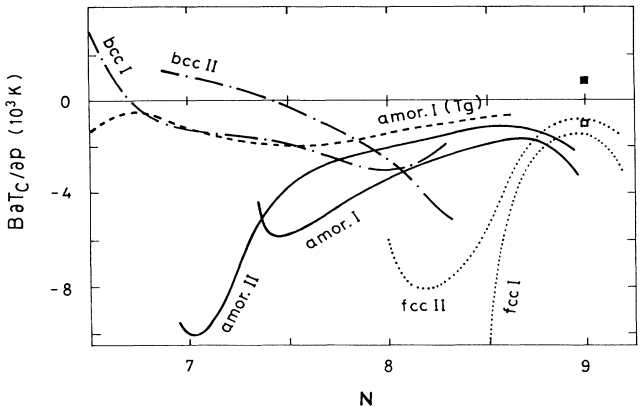

FIG. 10. Calculated $B\partial T_C/\partial p$ for amorphous (——), bcc (—·—·—·), and fcc (· · · ·) structures with the sets of input parameters of I ($\tilde{J}=0.059045$ Ry and W in Fig. 1) and II [$\tilde{J}=0.090$ Ry and $W/W(\mathrm{Fe})=0.441/0.393$]. Previous results for Ni with and without local electron correlations (Ref. 39) are shown by ■ and □, respectively. The results for $B\partial T_g/\partial p$ are also shown by a dashed curve.

the feedback effect which originates in the occurrence of competing ferro- and antiferromagnetic interactions; the LM's act to suppress the depolarization of surrounding LM's with increasing bandwidth near T_C. It should be noted that this is not necessarily characteristic of the structural disorder, as we see the same effect for the fcc structure in Fig. 10.

The pressure dependence of the SG temperature cannot be obtained by a phenomenological Heisenberg-type model because the volume dependence of exchange couplings is not known in the metallic systems. Present theory enables us to calculate $\partial T_g/\partial p$ since the theory is based on the microscopic Hamiltonian of the degenerate-band Hubbard model whose volume dependence is well known from the energy-band calculations. Calculated $\partial T_C/\partial p$ in Fig. 10 is not as sensitive to N in the range $6.5<N<7.5$, where the actual SG's are expected. The absolute values are comparable with the experimental data of Fe-rich amorphous alloys as will be discussed in the following section.

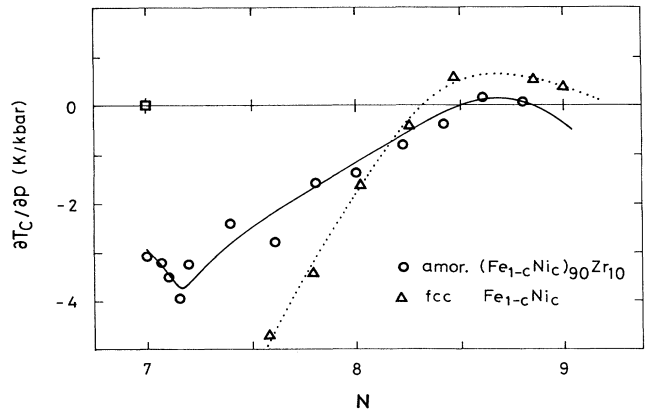

FIG. 11. Experimental data of $\partial T_C/\partial p$ for amorphous $(Fe\text{-}Ni)_{90}Zr_{10}$ (○) (Ref. 36), fcc Fe-Ni (△) (Ref. 37), and bcc FE (□) (Ref. 42).

V. MAGNETIC-FIELD AND PRESSURE EFFECTS IN THE REENTRANT SPIN GLASS

The most drastic change of magnetism with the magnetic field and pressure is expected to occur in the vicinity of ferromagnetic instability. We present here the magnetic-field and pressure effects in the reentrant SG regime ($7.350<N<7.385$), and discuss the experimental data for Fe-rich amorphous alloys near 90 at. % Fe.

A. High-field susceptibilities and forced volume magnetorestriction

Figure 12 shows the calculated results of the high-field susceptibilities (χ_{HF}) in the reentrant SG regime. Calculated χ_{HF} have huge values, which are 100 times as large as those in the crystalline Fe, Co, and Ni,[25] and show the temperature dependence consistent with the ac susceptibilities for amorphous Fe_cZr_{1-c} ($0.88\le c\le 0.92$) reentrant SG alloys.[6,10] The divergence at T_g is stronger than that at T_C. This is explained by the Curie-like enhancement of χ_{HF} at lower temperatures, which was caused by the paramagnetic component in the distribution $g(M)$. (See Fig. 14 in I.)

Recently, Tange, Tanaka, Goto, and Fukamichi have measured the forced volume magnetorestriction ($\partial\omega/\partial h$) of amorphous Fe_cZr_{1-c} ($0.88\le c\le 0.92$) alloys.[10] They found huge $\partial\omega/\partial h$ and an anomalous peak at T_g, which are not seen in the other SG systems. To throw light on this problem, we calculated $\partial\omega/\partial h$ by using the Liberman-Pettifor formula[43] (see the Appendix):

$$\frac{\partial\omega}{\partial h}=\frac{\dot{D}}{3BV}\frac{\partial E_b}{\partial h}=\frac{\dot{D}}{3BV}\left[T\frac{\partial[\langle m\rangle]_s}{\partial T}+\frac{1}{4}\tilde{J}\frac{\partial[\langle\xi^2\rangle]_s}{\partial h}\right]. \tag{5.1}$$

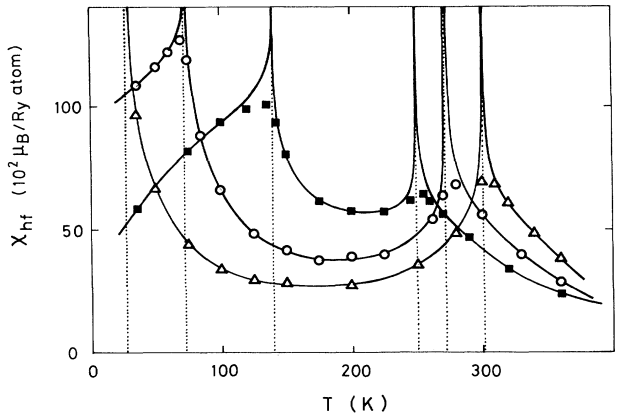

FIG. 12. High-field susceptibilities in the reentrant spin-glass region for $N=7.355$ (■), 7.365 (○), and 7.375 (△) obtained with the use of $h\approx 2.5\times10^{-5}$ Ry. The solid curves denote the values extrapolated to $h=0$.

Here E_b is the bonding energy [see Eq. (A2)]. $\dot{D}$ [=3.55 for Fe (Ref. 44)] is a proportionality constant given by the radial wave function at the Wigner-Seitz sphere.[45] The amplitude $[\langle \xi^2 \rangle]_s$ is directly related to the amplitude of LM as follows:[13]

$$[\langle \mathbf{m}^2 \rangle]_s = 3N - \frac{3}{2D}N^2 + \left[1+\frac{3}{2D}\right]\left[[\langle \xi^2 \rangle]_s - \frac{2}{\beta \tilde{J}}\right] . \tag{5.2}$$

Since the amplitudes $[\langle \xi^2 \rangle]_s$ are sensitive to the magnetic field h in the reentrant SG regime, $\partial[\langle \xi^2 \rangle]_s/\partial h$ are numerically calculated by applying finite field $h \approx 6\times 10^4$ $[G]$, and then obtained by an extrapolation to $h=0$. We present our results in Fig. 14. Calculated $\partial\omega/\partial h$ are very large as compared with those in the bcc Fe [0.05 [10^{-8} Oe^{-1}] (Ref. 46)] and fcc Ni [0.01 [10^{-8} Oe^{-1}] (Ref. 46)]. The results explain the order of magnitude and the divergence at T_g in the experimental data of amorphous Fe_cZr_{1-c} ($0.88 \le c \le 0.92$) alloys.[10]

According to Eq. (5.1), the forced volume magnetostrictions in the LM systems whose amplitudes hardly change with the magnetic field are determined by the temperature derivative of the magnetization [i.e., the first term on the rhs of Eq. (5.1)]. $\partial\omega/\partial h$ then diverge to plus infinity at T_g and to minus infinity at T_C. On the other hand, the Invar type of $\partial\omega/\partial h$ with soft amplitudes of the LM is determined by the second term on the rhs of Eq. (5.1). The present results of $\partial\omega/\partial h$ in the reentrant SG regime near amorphous Fe are dominated by the second term as shown by the dotted curve in Fig. 13 for $N=7.365$. In particular, a large peak at T_g is due to the variable amplitude of the LM. It should be noted that the contribution of the first term is less than only one-tenth or one-hundredth of the second one, and that the former is not expected to be large in any system. Therefore, the large anomaly of $\partial\omega/\partial h$ at T_g is a characteristic of the itinerant-electron SG, which is never seen in the insulator system.[12]

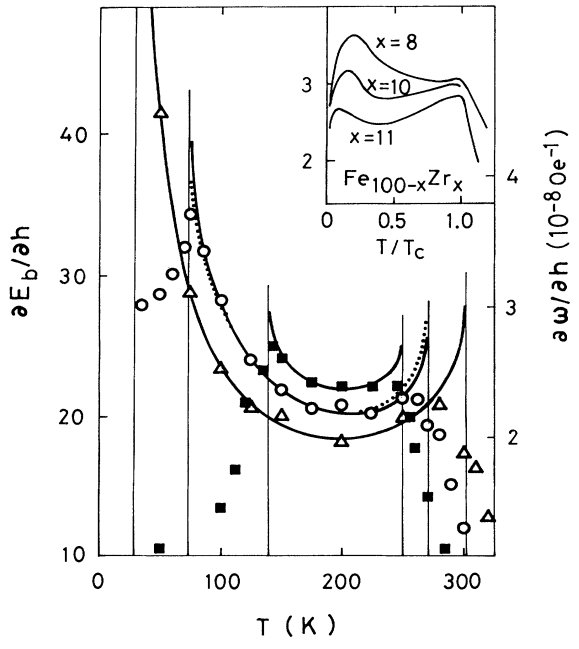

FIG. 13. Calculated $\partial E_b/\partial h$ and forced volume magnetorestrictions $\partial\omega/\partial h$ for $N=7.355$ (■), 7.365 (○), and 7.375 (△) with $h \approx 2.5\times 10^{-5}$ Ry, and those extrapolated to $h=0$. The inset shows the experimental data for amorphous Fe-Zr alloys (Ref. 10).

B. *T-P* phase diagram

Recent investigations by Goto *et al.*[11] have revealed that the amorphous Fe_cLa_{1-c} ($0.875 \le c \le 0.925$) alloys cause the pressure-induced ferromagnet-SG transition (see the inset of Fig. 16). Since the SG temperature around 90 at. % Fe hardly depend on the second elements, the basic aspect of the experimental data for amorphous Fe-La alloys may be expected to be explained only by the structural disorder. We therefore calculated the *T-p* phase diagram in the reentrant SG region.

Figure 14 shows the temperature dependence of the magnetization and the SG order parameter for $N=7.365$ when the bandwidth is varied. Both curves are similar to those expected from the Sherrington-Kirkpatrick model.[20] A calculated phase diagram is shown in Fig. 15. Calculated T_C decreases with increasing the bandwidth W, while reentrant T_g increases until the ferromagnetism disappears at a critical bandwidth or a critical pressure (p^*). This behavior explains the experimental phase diagrams in amorphous $Fe_{87.5}La_{12.5}$ and $Fe_{92.5}La_{7.5}$ alloys as shown in the inset of Fig. 15. (Note that the change of the bandwidth W is in proportion to the pressure for small values.) Calculated critical pressure p^*, $\partial T_C/\partial p$, and $\partial T_g/\partial p$ are summarized in Table III with the experimental values for amorphous $Fe_{87.5}La_{12.5}$ and $Fe_{92.5}La_{7.5}$ alloys.[11] The qualitative agreement between theory and experiment supports that the reentrant SG behavior near 90 at. % Fe is dominated by the structural disorder.

The reentrant SG shows a broad LM distribution as shown in Fig. 16, and the magnetism is determined by a detailed valence between the ferro- and antiferromagnetic couplings. The transition from the ferromagnetic to the SG state with increasing pressure is driven by a relative

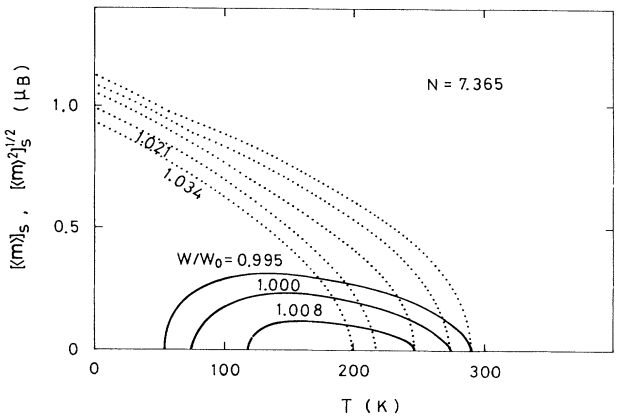

FIG. 14. Volume dependence of the magnetization (——) and SG order parameter (· · · ·).

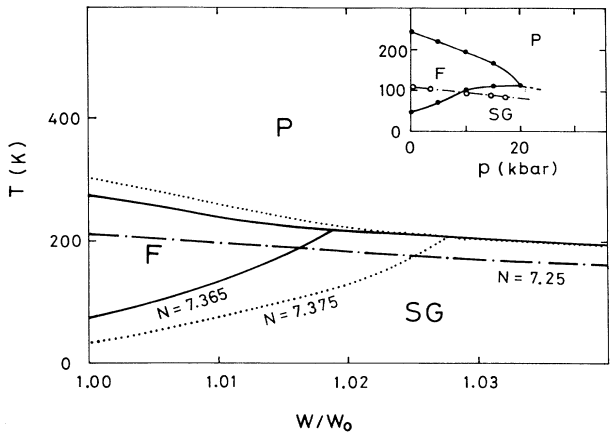

FIG. 15. T-W magnetic phase diagram showing ferromagnetic (F), spin-glass (SG), and paramagnetic (P) phases near the reentrant spin-glass region. W_0 denotes the d-band width at zero pressure. The inset shows the experimental data for amorphous $Fe_{87.5}La_{12.5}$ (●) and $Fe_{92.5}La_{7.5}$ (○) alloys (Ref. 11).

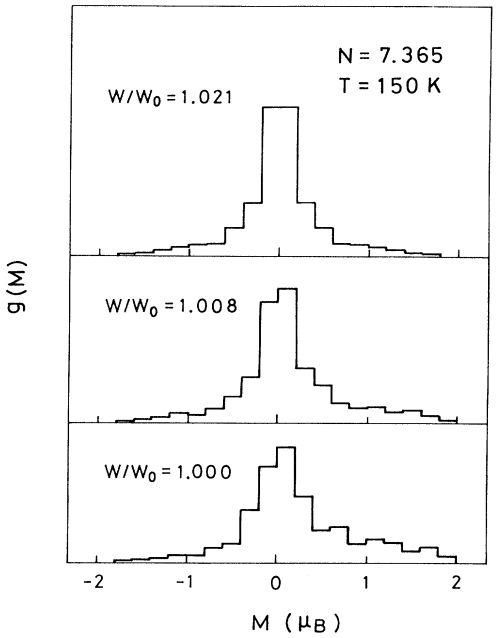

FIG. 16. Volume dependence of the LM distribution $g(M)$ for $N=7.365$.

change in the ratio of the short-range ferromagnetic couplings to the long-range antiferromagnetic couplings with decreasing volume.

VI. SUMMARY AND DISCUSSION

We have investigated the susceptibilities and the pressure effects of amorphous $3d$ transition metals on the basis of the finite-temperature theory of amorphous metallic magnetism. The structural disorder shifts the main peak of the DOS between the bcc and fcc ones, and causes the fluctuations $[\langle m\rangle^2]_s-[\langle m\rangle^2]_s$. The former produces the strong ferromagnetism near $N^*=8.353$, while the latter causes the SG near amorphous Fe. Calculated paramagnetic susceptibilities for amorphous structure therefore show the largest value among the amorphous, bcc, and fcc structures for the d electron number $8.0<N<8.5$. The effective Bohr-magneton numbers take the smallest values for $7.80<N<8.85$. The pressure dependence of amorphous $|\partial M/\partial p|$ and $|\partial T_C/\partial p|$ has also been shown to be small in the same region because of the strong ferromagnetism.

When the d electron number is decreased from $N^*=8.353$, $m_{\rm eff}$, $|\partial M/\partial p|$, and $|\partial T_C/\partial p|$ increase because of the gradual transition from the strong to weak ferromagnetism. Finally, the high-field susceptibility diverges at $N=7.385$, although $\partial T_C/\partial p$ is suppressed there because of the feedback effect. The Invar anomalies in amorphous metals occur near amorphous Fe ($N\approx 7.0$) rather than the average electron number found in the fcc Invar alloys ($N=7.7$), which is attributed to the difference in the main-peak position between the amorphous and fcc structures.

The structural disorder causes the SG state after disappearance of ferromagnetism. We have shown that the present theory with structural disorder qualitatively or

TABLE III. Critical pressure p^* and pressure dependence of magnetization M, Curie temperature T_C, and SG temperature T_g in the reentrant SG region. Bulk modulus for amorphous $Fe_{87}B_{13}$ (Ref. 48) was used in the calculations.

	p^* (kbar)	$\partial M/\partial p$ (μ_B/kbar)	$\partial T_C/\partial p$ (K/kbar)
Theory ($N=7.365$)	12	−2.2	−5.3
($N=7.375$)	18	−2.1	−6.4
Expt.	20[a]	−2.8[b]	−5.1[a]
	($Fe_{87.5}La_{12.5}$)	($Fe_{90}Ce_{10}$)	($Fe_{87.5}La_{12.5}$)
			$\partial T_g/\partial p$ (K/kbar)
Theory ($N=7.0$)			−1.5
($N=7.25$)			−2.1
Expt.			−1.4[a]
			($Fe_{92.5}La_{7.5}$)

[a]Goto *et al.*, Ref. 11.
[b]Komatsu and Fukamichi, Ref. 47.

semiquantitatively explains χ, $\partial\omega/\partial h$, and the T-P phase diagram in the amorphous Fe-La and Fe-Zr reentrant SG around 90 at. % Fe. This supports the previous conclusion that the SG's in Fe-rich amorphous alloys at more than 90 at. % Fe are the itinerant-electron SG produced by the structural disorder.[9,49] In particular, we found that the anomalous divergence of $\partial\omega/\partial h$ at the reentrant T_g is a characteristic of the itinerant-electron SG which is not expected in the insulator SG systems.

Very recently, Tanaka, Takayama, and Fujiwara[50] verified on the basis of the first-principles linear muffin-tin orbital (LMTO) recursion method that the amorphous Co certainly has the Fermi level just at the main peak in the nonmagnetic DOS, and showed a strong ferromagnetism at the ground state. This result supports our picture for strong ferromagnetism in amorphous $3d$ transition metals. Systematic ground-state calculations with use of the first-principles LMTO-recursion method[51] or the LMTO supercell approach[52] are highly desired to establish the electronic structure assumed in this work for $3d$ amorphous transition metals and alloys.

From the experimental point of view, the enhancement of the ferromagnetism near $N^*=8.353$ in the amorphous structure seems to be realized in amorphous Fe_cNi_{1-c} ($0.64\le c\le 0.72$) alloys[53] because the amorphous Fe_cNi_{1-c} alloys show strong hyperfine fields in the region $0.64\le c\le 0.72$, in contrast to the crystalline Fe-Ni Invar alloys in which a sharp drop of the hyperfine field is well known to occur. Hasegawa and Mizutani[54] have recently performed the systematic investigations for Co-based amorphous alloys. They observed a tendency that the spin-wave stiffness constant obtained from magnetization -temperature curves rapidly increase going beyond the value of hcp pure Co with increasing Co concentration. Their results also support the enhancement of the ferromagnetism near $N^*=8.353$.

Systematic measurements of susceptibilities are left for a future task. The investigations with use of other experimental techniques are also required to clarify the magnetic properties of amorphous metallic magnetism. Direct measurements of the stiffness constant by means of the neutron-diffraction experiment would be useful to verify the enhancement of magnetic couplings near N^*. The shift of the main peak of about 0.4 eV in the DOS might be observed directly by means of the photoemission and inverse photoemission experiments in the nonmagnetic $3d$ and $4d$ transition metals and alloys. We hope that these experimental efforts will establish the basic picture for the physics of amorphous transition metals and alloys in the near future.

ACKNOWLEDGMENTS

The author would like to thank Professor K. Fukamichi, Professor T. Goto, Dr. T. Hasegawa, Dr. H. Komatsu, Professor U. Mizutani, and Professor H. Tange for informing him of their experimental data prior to publication. He also thanks Dr. H. Tanaka for sending him the DOS for amorphous Co prior to publication. He is much indebted to Professor J. M. D. Coey, Dr. S. Ishio, Dr. I. Renz, Professor E. F. Wassermann, and Dr. M. Yu for valuable discussions. This work was partly supported by a Grant-in-Aid for Scientific Research from the Ministry of Education, Science, and Culture in Japan.

APPENDIX: DERIVATION OF Eq. (5.1)

The forced volume magnetorestriction $\partial\omega/\partial h$ is calculated from pressure p as follows:

$$\frac{\partial\omega}{\partial h}=\frac{1}{3BV}\frac{\partial(3pV)}{\partial h}\ . \tag{A1}$$

According to the Libermann-Pettifor virial theorem [Eq. (A4) in Ref. 45] the electronic contribution to the pressure (p_e) is given by

$$3p_eV=\sum_i C_i\langle n_i\rangle+\dot{D}\left\langle\sum_{ivjv'\sigma} t_{ivjv'}a^{\dagger}_{iv\sigma}a_{jv'\sigma}\right\rangle\ . \tag{A2}$$

Here we take into account the d orbitals only. C_i and $\dot{D}$ are the volume-dependent coefficient for the core part (the first term on the rhs) and the volume-independent coefficient for the bonding energy part (the second term), respectively, both of which are obtained from the LMTO method.[44] $t_{ivjv'}$ in Eq. (A2) is the transfer integral between the orbital v on site i and the orbital v' on site j. $a^{\dagger}_{iv\sigma}$ ($a_{iv\sigma}$) denotes the creation (annihilation) operator for an electron with spin σ on site i and orbital v, and $n_i=\sum_{v\sigma}a^{\dagger}_{iv\sigma}a_{iv\sigma}$.

We adopt the degenerate-band Hubbard model with the Coulomb integral U and the Hund's rule coupling J as follows:

$$H=\sum_i(\epsilon_i-h\sigma)n_{i\sigma}+\sum_{ivjv'\sigma}t_{ivjv'}a^{\dagger}_{iv\sigma}a_{jv'\sigma}+\frac{1}{4}\sum_i(Un_i^2-J\mathbf{m}_i^2)\ . \tag{A3}$$

Here ϵ_i denotes the atomic level on site i.

Substituting the bonding energy [the second term on the rhs of Eq. (A3)] obtained from the above Hamiltonian into Eq. (A2), and taking the derivative of Eq. (A2) with respect to h at $h=0$, we reach

$$\frac{\partial(3p_eV)}{\partial h}=\dot{D}\left[T\frac{\partial M}{\partial T}-\frac{1}{4}\sum_i\left[U\frac{\partial\langle n_i^2\rangle}{\partial h}-J\frac{\partial\langle\mathbf{m}_i^2\rangle}{\partial h}\right]\right]\ . \tag{A4}$$

Here we used the relation $\partial\langle H\rangle/\partial h=-M+T\partial M/\partial T$, M being the total magnetization.

In the two-field static approximation, the amplitude of the LM, and the square of local charge are given by

$$\langle n_i^2\rangle=\langle n_i\rangle+\left[1-\frac{1}{2D}\right]\langle n_i\rangle^2-\frac{1}{2D}\left[\langle\xi_i^2\rangle-\frac{2}{\beta\tilde{J}}\right]\ , \tag{A5}$$

$$\langle\mathbf{m}_i^2\rangle=3\langle n_i\rangle-\frac{3}{2D}\langle n_i\rangle^2+\left[1+\frac{1}{2D}\right]\left[\langle\xi_i^2\rangle-\frac{2}{\beta\tilde{J}}\right] \tag{A6}$$

in the charge neutrality limit.[13]

Substitution of Eqs. (A5) and (A6) into Eq. (A4) leads to the following expressions:

$$\frac{\partial(3p_e V)}{\partial h}=\dot{D}\left[T\frac{\partial M}{\partial T}+\frac{1}{4}\sum_i \tilde{J}\frac{\partial\langle \xi_i^2\rangle}{\partial h}\right] \tag{A7}$$

and

$$\tilde{J}=\frac{1}{2D}U+\left[1+\frac{1}{2D}\right]J\ . \tag{A8}$$

We reach Eq. (5.1) substituting Eq. (A7) into Eq. (A1) and taking the structural average.

[1]F. E. Luborsky, in *Ferromagnetic Materials,* edited by K. H. J. Bushow and E. P. Wohlfarth (North-Holland, Amsterdam, 1980), Vol. 1, p. 451.

[2]K. Moorjani and J. M. D. Coey, *Magnetic Glasses* (Elsevier, Amsterdam, 1984).

[3]T. Mizoguchi, in *Magnetic and Magnetic Materials 1976 (Joint MMM-Intermag Conference, Pittsburgh),* Partial Proceedings of the First Joint MMM-Intermag Conference, AIP Conf. Proc. No. 34, edited by J. J. Becker and G. H. Lander (AIP, New York, 1976), p. 286.

[4]K. Fukamichi, T. Goto, H. Komatsu, and H. Wakabayashi, in *Proceedings of the Fourth International Conference on the Physics of Magnetic Materials,* edited by W. Gorkowski, K. Lachowicz, and H. Szymczak (World Scientific, Singapore, 1989), p. 354.

[5]H. Hiroyoshi and K. Fukamichi, J. Appl. Phys. **53**, 2226 (1982).

[6]N. Saito, H. Hiroyoshi, K. Fukamichi, and Y. Nakagawa, J. Phys. F **16**, 911 (1986).

[7]J. M. D. Coey, F. Givord, A. Lienard, and J. P. Reboulat, J. Phys. F **11**, 2707 (1981); D. H. Ryan, J. M. D. Coey, E. Batalla, Z. Altonian, and J. O. Strom-Olsen, Phys. Rev. B **35**, 8630 (1987).

[8]K. Fukamichi, T. Goto, and U. Mizutani, IEEE Trans. Magn. Mag-**23**, 3590 (1987).

[9]Y. Kakehashi, Phys. Rev. B **43**, 10 820 (1991).

[10]H. Tange, Y. Tanaka, M. Goto, and K. Fukamichi, J. Magn. Magn. Mater. **81**, L243 (1980).

[11]T. Goto, C. Murayama, N. Mori, H. Wakabayashi, K. Fukamichi, and H. Komatsu, J. Phys. (Paris) Colloq. **49**, C8-1143 (1988).

[12]Y. Kakehashi, J. Magn. Magn. Mater. **103**, 78 (1991).

[13]Y. Kakehashi, Phys. Rev. B **34**, 3243 (1986).

[14]Y. Kakehashi, Phys. Rev. B **41**, 9207 (1990).

[15]A. Bieber and F. Gautier, Solid State Commun. **39**, 149 (1981); T. Oguchi, K. Terakura, and N. Hamada, J. Phys. F **13**, 145 (1983).

[16]F. Matsubara, Prog. Theor, Phys. **52**, 1124 (1974); S. Katsura, S. Fujiki, and S. Inawashiro, J. Phys. C **12**, 28739 (1979).

[17]J. Hubbard, Phys. Rev. B **19**, 2626 (1979); **20**, 4584 (1979); **23**, 597 (1981).

[18]H. Hasegawa, J. Phys. Soc. Jpn. **46**, 1504 (1979); **49**, 178 (1980).

[19]S. F. Edwards and P. W. Anderson, J. Phys. F **5**, 965 (1975).

[20]D. Sherrington and S. Kirkpatrick, Phys. Rev. Lett. **35**, 1972 (1975).

[21]R. Yamamoto and M. Doyama, J. Phys. F **9**, 617 (1979).

[22]M. Matsuura, H. Wakabayashi, T. Goto, H. Komatsu, and K. Fukamichi, J. Phys. Condens. Matter **1**, 2077 (1989).

[23]T. Fujiwara, Nippon Butsuri Gakkaishi **40**, 209 (1985).

[24]V. L. Moruzzi, J. F. Janak, and A. R. Williams, *Calculated Electronic Properties of Metals* (Pergamon, New York, 1978).

[25]J. P. Rebouillat, TEEE Trans. Magn. Mag. **8**, 630 (1972).

[26]Y. Nakagawa, J. Phys. Soc. Jpn. **11**, 855 (1956); **12**, 700 (1957).

[27]Sucksmith and R. R. Pearce, Proc. R. Soc. London, Ser. A **167**, 189 (1938).

[28]M. Fallot, J. Phys. Radium **5**, 153 (1944).

[29]Y. Kakehashi, Prog. Theor. Phys. Suppl. **101**, 105 (1990).

[30]I. Renz and S. Methfessel, J. Phys. (Paris) Colloq. **49**, C8-119 (1988).

[31]U. K. Poulsen, J. Kollár, and O. K. Andersen, J. Phys. F **6**, L241 (1976).

[32]J. S. Kouvel and R. H. Wilson, J. Appl. Phys. **32**, 435 (1961).

[33]J. S. Kouvel and C. Hartelius, J. Phys. Chem. Solids **25**, 1357 (1964).

[34]H. Ebert and A. Kussmann, Z. Phys. **38**, 437 (1937).

[35]H. Tange, Y. Tanaka, and K. Shirakawa, J. Phys. (Paris) Colloq. **49**, C8-1281 (1988).

[36]H. Tange, Y. Tanaka, T. Kamimori, and M. Goto, J. Phys. (Paris) Colloq. **49**, C8-1283 (1988).

[37]J. M. Leger, C. Loriers-Susse, and B. Vodar, Phys. Rev. B **6**, 4250 (1972).

[38]Y. Kakehashi and P. Fulde, Phys. Rev. B **32**, 1595 (1985).

[39]Y. Kakehashi, Phys. Rev. B **38**, 6928 (1988).

[40]K. Fukamichi, M. Kikuchi, S. Arakawa, and T. Masumoto, Solid State Commun. **23**, 955 (1977).

[41]K. Fukamichi and H. Hiroyoshi, Sci. Rep. RITU A **32**, 154 (1985).

[42]L. Patrick, Phys. Rev. **93**, 384 (1954).

[43]Y. Kakehashi, Physica B **161**, 143 (1989).

[44]Y. Kakhashi, J. Phys. Soc. Jpn. **50**, 792 (1981).

[45]Y. Kakehashi, J. Phys. Soc. Jpn. **50**, 1925 (1981).

[46]J. L. Snoek, Physica **4**, 853 (1937).

[47]H. Komätsu and K. Fukamichi (unpublished).

[48]A. Tomizuka, H. Iwasaki, K. Fukamichi, and T. Kikegawa, J. Phys. F **14**, 1507 (1984).

[49]Y. Kakehashi, Phys. Rev. B **40**, 11 059 (1989).

[50]H. Tanaka, S. Takayama, and T. Fujiwara J. Phys. Condens. Matter (to be published).

[51]H. J. Nowak, O. K. Andersen, T. Fujiwara, and O. Jepsen, Phys. Rev. B **44**, 3577 (1991); Sonia Frota-Pessoa, *ibid.* **46**, 14 570 (1992).

[52]S. K. Bose, S. S. Jaswal, and O. K. Andersen, Phys. Rev. B **37**, 9955 (1988).

[53]J. Arai, J. Appl. Phys. **64**, 3143 (1988).

[54]T. Hasegawa and U. Mizutani (unpublished).